

# Synthesis and Characterization of Mn-Zn soft ferrite nanoparticle of Gd<sup>3+</sup> doped

Indu Sharma<sup>1</sup>, Pankaj Kumar<sup>1</sup>

Department of Physics, Career Point University, Hamirpur, Himachal Pradesh, India<sup>1</sup>,

## Abstract

*Manganese-Zinc Ferrite is a very high permeability magnetic material. The permeability is depended on the amount of manganese and zinc used in the synthesis of ferrite material. Reagent graded raw materials were used as initial material to synthesize and get a characterization of Mn-Zn based spinel ferrite. The nanocrystalline powders of manganese ferrite were obtained by the process of citrate precursor method. The obtained nanocrystals of Mn-Zn were doped by Gadolinium which further it was employed to produce specimens of  $Mn_{0.5}Zn_{0.5}Gd_xFe_{2-x}O_4$  ( $x = 0, 0.01, 0.03$ ). The study of doped (Gd) Mn-Zn ferrite nanocrystals was characterized by X-ray diffraction (XRD) and scanning electron microscopy (SEM). The results of XRD data determine the average crystallite size of doped (GD) Mn-Zn nanocrystals in the range of 40nm to 45nm. The images obtained through FE-SEM shows the flake-like structure of doped (Gd) Mn-Zn ferrite nanocrystals. Further studies of doped (Gd) Mn-Zn ferrite were done by FTIR and Raman spectroscopy.*

**Keyword:** Nanoparticle, Ferrite, Structural, Morphological and Spectroscopy properties

## 1. Introduction

Nanoparticles are the particle of size between 1 nanometer to 100 nanometer. Nanoscience and nanotechnology are the two terms related to nanoparticles. Nanoscience is defined as the study of the phenomena and the manipulation of the material at atomic, molecule scale, whereas nanotechnology is design, functionalization, characterization, and make use of the material at the nanometer scale. So in the field of nanotechnology, the nanoparticles are typically in the size range between 1-100 nm. Nanoparticles are confidential according to their diameter. Properties of ferrites are recognized to be sensitive to the processing technique [1-2]. A small deviation in the compositional stoichiometric of the ferrite affects its properties greatly. Soft ferrites such as Mn-Zn are well-known ferrites covering wide-ranging applications [3-4]. Mn-Zn ferrites are very important soft magnetic materials because of their high initial magnetic permeability, saturation magnetization, electrical resistivity, and low power losses [5]. Among various spinel ferrites, Mn-Zn ferrites are useful ceramic magnetic materials due to low core losses at high frequencies, high initial magnetic permeability, and high resistance [6-7]. The magnetic properties of Mn-Zn ferrites depend upon elemental composition, synthesis conditions, crystal structure, microstructure, sintering temperature, particle size, sintering time and shape of particles [8]. These materials are extensively used as inductors, transformers, antenna rods, loading coils, deflection yokes, choke coils, recording

heads, magnetic amplifiers, electromagnetic interference devices (EMI), power transformers and splitters. Besides, Mn–Zn ferrites are very important in biomedicine as magnetic carriers for bio-separation, enzymes, and proteins immobilization. Ferromagnetic materials are magnetic ceramics which are used to assemble many devices such as permanent magnets, memory storing devices, and microwave machines and for the telecommunication machines function. Spinel ferrites have been researched for their magnetic and electrical properties. In the spinel crystal structure, the oxygen ions form a cubic close-packed range in which two types of interstice occur, one synchronized tetrahedrally and the other octahedrally with oxygen ions. The unit cell shown in the figure is seen to be made up of octants, four containing one type of structure (shaded), and four containing another (unshaded). In this image some of the A-site cations lie at the corners and face-center positions of the large cube; a tetrahedral and an octahedral site are shown. The close-packed layers of the oxygen ion lattice lie at right angles to the body diagonal body [9-10]. In a spinel structure, both divalent and trivalent cations are dispersed among tetrahedral (A) and octahedral (B) sites. The site preference exhibited by divalent ions defines whether the spinel is normal, inverse, or mixed. In normal spinel, the  $A^{2+}$  ions occupy only tetrahedral sites and the  $B^{3+}$  ions occupy only octahedral sites. In inverse spinel, all the  $A^{2+}$  ions and half of the  $B^{3+}$  ions sit on the octahedral sites; the tetrahedral sites are occupied now by the other half of the  $B^{3+}$  ions. In most cases, magnetic divalent cations such as  $Mn^{2+}$  preferred at octahedral sites and manufacture an inverse spinel structure. A variety of synthetic ferrites were prepared by Hilpert in 1909 by using the precursor method, who suggested the basic formula for ferrites as  $MFe_2O_4$ , where M is a divalent metal ion [11]. The citrate precursor method was used to fine control the cation stoichiometric and the particle size. Dielectric and magnetic properties of Mn-Zn ferrite obtain by citrate precursor method were investigated. We have also investigated the influence of the atmosphere of the calcination process taking place the crystalline structure of Mn–Zn ferrite. In sequence to obtain good quality ferrites with reproducible stoichiometric composition and preferred microstructure, the citrate precursor method [12]. In this work, we considered the effect of Gd-substitution on phase formation and magnetic properties. It creates that small substitution of  $Fe^{3+}$  ions by  $Gd^{3+}$  ions may usefully influence the electromagnetic properties of ferrites facilitating good magnetic characteristics for high-frequency applications [13]. The rare-earth materials are strongly paramagnetic, but several of them ferromagnetic at low temperatures except for gadolinium ions.  $Gd^{3+}$  ions if possible enter octahedral B-sites. Substitution of the  $Gd^{3+}$  ions in spinel ferrites is recognized to decrease the saturation magnetization because of its paramagnetic nature at room temperature and lower magnetic moment as compared to ferromagnetic  $Fe^{3+}$  ions.

## 2. Materials and methods

### 2.1 Synthesis of $MnZnFe_2O_4$ nanoparticle

All the chemicals used in this study are of systematic reagent grade manganese (II) nitrate hexahydrate [ $Mn(NO_3)_2 \cdot 4H_2O$ ] (98%), Zinc nitrate hexahydrate [ $Zn(NO_3)_2 \cdot 6H_2O$ ] (96%), ferric (III) nitrate monohydrates ( $Fe(NO_3)_3 \cdot 9H_2O$ ) (99%), Citric Acid [ $C_6H_8O_7 \cdot H_2O$ ] and Gadolinium oxide [ $Gd_2O_3$ ] (99.9%) were used as initial materials. The metal nitrates were

dissolved simultaneously in a minimum amount of deionized water about 100 ml to get a clear solution. The metal nitrates precursor solution was added with citric acid under continuous stirring. The entire reaction was carried out at 60°C.  $\text{Fe}(\text{NO}_3)_3 \cdot 9\text{H}_2\text{O}$  (analytical grade),  $\text{Mn}(\text{NO}_3)_2 \cdot 4\text{H}_2\text{O}$  (98% pure),  $\text{Zn}(\text{NO}_3)_2 \cdot 6\text{H}_2\text{O}$  (96% pure), and  $\text{C}_6\text{H}_8\text{O}_7 \cdot \text{H}_2\text{O}$  (hydrated citric acid) were used as starting materials in the present study. The iron nitrate, manganese nitrate, and zinc nitrate were combined to yield a composition with the general formula  $(\text{Mn-Zn})\text{FeO}$ . A stoichiometric amount of metal nitrates and a suitable quantity of citric acid was dissolved in deionized water with the ratio 1: 1 of nitrate to citrate. The pH of starting solutions was adjusted in the range of 5-7. After a mixed solution was heated at 50°C and continuously. The precursor was then calcined at varying temperatures from 1200°C for 2 h in a muffle furnace. The crystal structures of the Mn-Zn ferrite powders were examined via x-ray diffraction (XRD) studies using an X-ray diffractometry. The XRD pattern analysis was performed to determine the chemical purity and phase homogeneity of the prepared powders. The morphology and crystalline of particles were investigated with scanning electron microscopy.

### 3. Results and discussion

#### 3.1 X-ray diffraction (XRD) results

The patterns are indexed according to the standard procedure of indexing of the XRD pattern. The X-Ray diffraction graphs show the peaks with corresponding crystallographic planes. The obtained pattern is not phased pure as impurity phases are also associated with the spinel structure. The crystallographic information includes lattice parameters and crystallite sizes. To make practically usable calcined powders have been compacted into pellets and sintered at varying temperatures to see the phase stability. XRD result has been analyzed with matching with the standard pattern from research paper  $\text{Gd}^{3+}$  doped Mn-Zn soft ferrite nanoparticle. The results have been discussed with the XRD pattern along with lattice parameters and crystallite sizes. XRD spectra of  $\text{Mn}_{0.5}\text{Zn}_{0.5}\text{Gd}_x\text{Fe}_{2-x}\text{O}_4$  ( $x = 0, 0.01, 0.03$ ) pre-sintered at 500°C and sintered at 1250°C samples comprises of (111), (220), (112), (311), (222), (333), (511), (440) and (533) planes (**Fig.3.1**) conformed the formation the spinel structure cubic manganese zinc ferrite with no other phases or impurities. The presence of these planes confirms that  $\text{Gd}^{3+}$  doped Mn-Zn ferrites have a pure spinel structure. The most well-known peak corresponding to a plane (311) has been found to shift towards a higher angle with the addition of  $\text{Gd}^{3+}$  content.

This most prominent peak i.e. the maximum number of the orientation of corresponding to a plane (311) and has been used to estimate crystallite size. The average crystalline size of sintered  $\text{Mn}_x\text{Zn}_x\text{Gd}_x\text{Fe}_{2-x}\text{O}_4$  ( $x = 0.0, 0.01, 0.03$ ) ferrites samples was found to be 44.22, 42.96 and 40.54 nm respectively. The average crystalline size was 38 nm with maximum intensity Table (3.1) shows the value of average crystalline size (D), interplanar spacing ( $d_{hkl}$ ), and lattice constant (a, b and c, as crystal structure is cubic:  $a=b=c$ ) with an increase in sintering temperature were calculated by using Braggs equations and Scherer formula.

Crystalline size (D), Lattice constant (a), interplanar spacing (d), and packing factor (P) have been determined using equations 1, 2, 3, and 4 respectively. Nanoparticles were determined by using Debye Scherer’s relation.

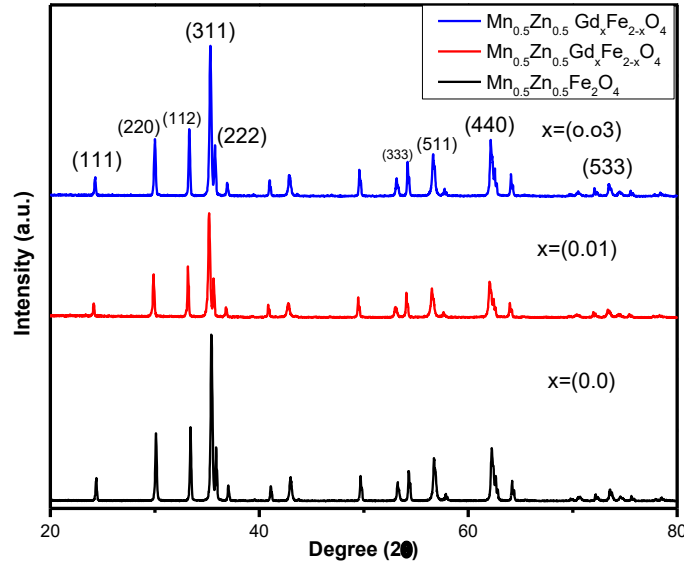


**Figure 3.1:**XRD graphs of  $Mn_xZn_xGd_xFe_{2-x}O_4$  ( $x = 0.0, 0.01, 0.03$ ) ferrites

$$D = K \lambda / \beta \cos\theta \dots\dots\dots [1]$$

$$a = d (h^2 + k^2 + l^2)^{1/2} \dots\dots\dots [2]$$

$$d = 2d \sin\theta / n\lambda \dots\dots\dots [3]$$

$$p = D/d \dots\dots\dots [4]$$

Where D = Crystalline size, K = Debye Scherer constant (0.9),  $\lambda$  = Wavelength of light (1.546 Å for  $K\alpha$ ),  $\beta$  = Full-width at half maximum of the peaks and  $\theta$  = Diffraction angle, a = Edges of the cube, d = Interplaner spacing, n = Order of the reflection, p = Packing fraction and h, k, l are the miller indices of cubic structure.

The values of crystallite size, the lattice constant, interplanar spacing and packing factor has been given in Table 3.1. It has been observed that the values of crystallite size, the lattice constant, inter planer spacing, and packing factor decreases with the increase of Gd content in Mn-Zn ferrites. The decrease in these structural parameters may be due to the difference in the ionic radii of rare-earth ions and  $Fe^{3+}$  ions.

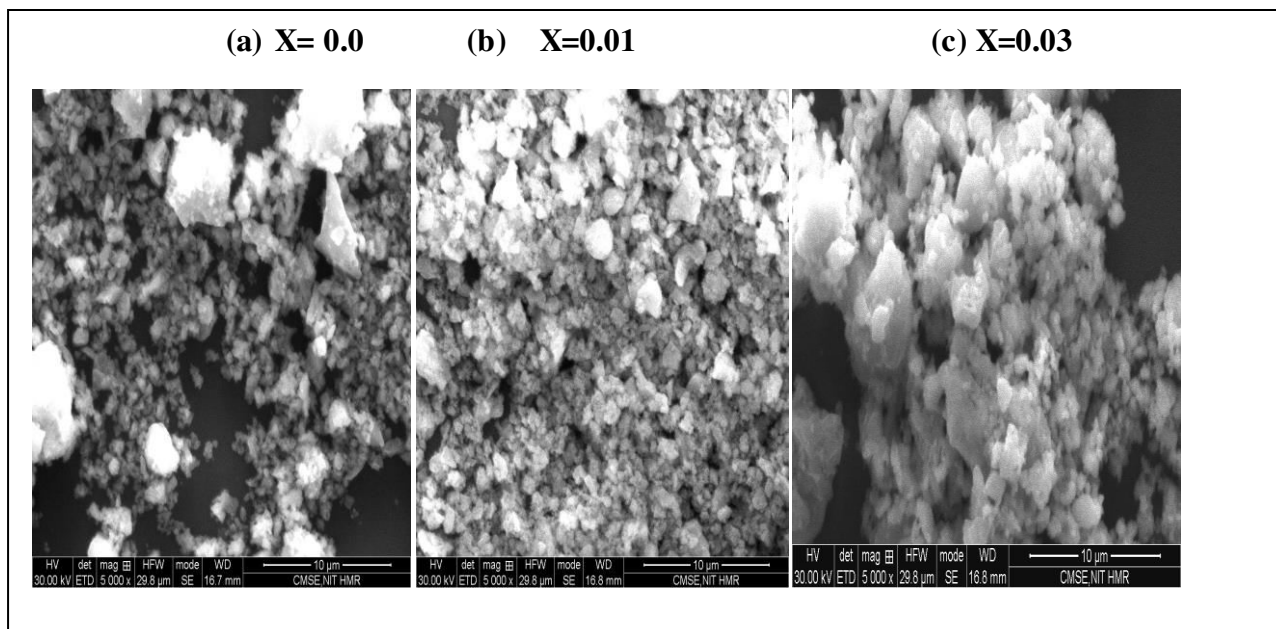
**Table 3.1:** Values of crystallite size (D), interplanar spacing (d), lattice constant (a) and packing factor (P) for  $Mn_{0.5}Zn_{0.5}Gd_xFe_{2-x}O_4$  ( $x = 0, 0.01, 0.03$ ) ferrites

$Mn_xZn_xGd_xFe_{2-x}O_4$	D (nm)	d (Å)	a (Å)	P
x = 0.0	44.22	2.546	8.444	174.09

$x = 0.01$	42.96	2.578	8.477	166.64
$x = 0.03$	40.54	2.555	8.552	158.66

### 3.2 Scanning Electron Microscope (SEM) results

SEM image of Gadolinium substituted Manganese zinc ferrites with the composition are shown in Fig. 3.2 (a) (b) (c). The samples were studied by placing these under a scanning electron microscope. SEM micrographs have been used to investigate the morphological study of the nano ferrites. SEM images of the nano ferrites were given at a scale of 3, 5, and 10 $\mu$ m for synthesized material. SEM micrograph, given Fig. 4.2 containing all the three sample images represent that the particles grains are defined faceted and flakes like structure. However, the close examination of the images shows that particles are distorted rhombus, cuboidal, and trigonal in shape. Sharp boundaries of grains suggest that there is no liquid phase after sintering. The particles of the  $Mn_{0.5}Zn_{0.5}Gd_xFe_{2-x}O_4$  ( $x = 0.03$ ) ferrites examine using “Image J” software found to befall in the range of 45-200nm, however, the side of the rhombus/trigonal is approximately 60nm in average. The particles of  $Mn_{0.5}Zn_{0.5}Gd_xFe_{2-x}O_4$  ( $x = 0.01$ ) ferrites fall in the range of 80-220nm, having the average side length of approximately 90nm. Furthermore, the particles of  $Mn_{0.5}Zn_{0.5}Fe_{2-x}O_4$  ( $x = 0$ ) ferrites are a little bit bigger and the particles fall in the range of 118-430 nm having the trigonal and cuboidal shape particles. These results conclude that lowering the Gd content in Mn-Zn ferrites increases the particle size of the ferrites.



FTIR spectra MnZnFe<sub>2</sub>O<sub>4</sub> sample recorded in the range 4000-400 cm<sup>-1</sup> are shown in Fig 3.3 When the mixture of citric acid (CA) is additional absorption peaks appear in the FTIR spectra at 3422 cm<sup>-1</sup>. Microstructure (larger magnification) of ferrite powders prepared from citric acid. The FTIR spectra of  $Mn_xZn_{1-x}Gd_xFe_2O_4$  ( $x = 0.0, 0.01, 0.03$ ) are shown in Fig.4.

The tetrahedral and octahedral vibration frequencies ( $\nu_1$  and  $\nu_2$ ) listed in Tab.3.3. It was observed that both tetrahedral and octahedral vibrational frequencies are shifted towards the higher frequencies with an increase in  $\text{Mn}^{2+}$  ion concentration, which is ascribed to an increase in force constants and contraction of  $\text{Fe}^{3+} - \text{O}_2^-$  bond lengths at both A and B sites. This supports the observed decrease in lattice constant. T. Slatineanu et al. observed a similar variation in Zn ferrites substituted with Ni. M.A. Gabal et al. reported an increase in  $\nu_1$  and random.

The increase in  $\nu_1$  and  $\nu_2$  in the present series attributed to the random distribution of cations in tetrahedral (A) and octahedral (B) sites against their normal preference. The band with the higher wavenumber observed in the range 632-646  $\text{cm}^{-1}$  corresponding to the intrinsic stretching vibration of the metal at the tetrahedral site. The broadband around O-H stretching vibration peak 3322  $\text{cm}^{-1}$  can be assigned to the hydroxyl group and the bands around 1639-1374  $\text{cm}^{-1}$  C=O stretching vibration peak. The other band around the range 404-416 is attributed to the octahedral metal stretching confirming the formation of inverse spinel  $\text{MnZnFe}_2\text{O}_4$  and 1116  $\text{cm}^{-1}$  can be assigned to C-O stretching vibration peak.

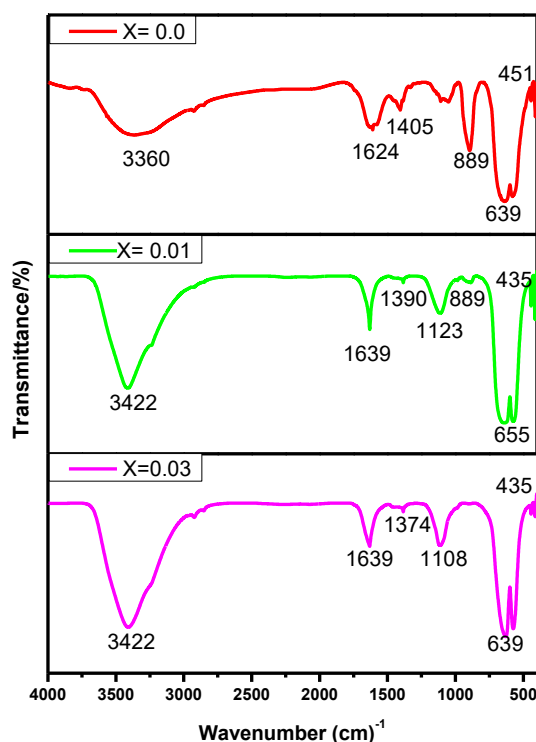


**Figure 3.3:** FTIR spectra of  $\text{Mg}_x\text{Zn}_{1-x}\text{Gd}_x\text{Fe}_2\text{O}_4$ , ( $x = 0.0, 0.01, 0.03$ )

**Table 3.3:** Tetrahedral, octahedral vibration frequencies  $\nu_1$  and  $\nu_2$

X	$\nu_1$ ( $\text{cm}^{-1}$ )	$\nu_2$ ( $\text{cm}^{-1}$ )
0.0	632	404

0.01	632	408
0.03	646	416

### 3.4 Raman spectroscopy

Raman studies of the synthesized Mn–Zn nano-ferrite samples were carried out by recording the Raman spectra (Fig.3.4) at room temperature at frequencies from 100 to 1000  $\text{cm}^{-1}$ . Raman spectroscopy is an important and powerful technique for analysis of the structural and vibrational characteristics of materials. To determine the natural tendency of the frequency, line width, and lattice effect in all three synthesized samples. The spectra of Mn–Zn nano ferrites consist of broadband of nearly at 227, 304, 408, 561, 561,711  $\text{cm}^{-1}$  of which the 707  $\text{cm}^{-1}$  is the broadest band Gupta et al. Assignment of these active Raman modes took into account the facts that  $\text{MnZnFe}_2\text{O}_4$  is a partially inverse spinel structure that belongs to the space group  $\text{Da}$  Silva SW et al. The lightest ion  $\text{Mn}^{2+}$  responds for the Raman mode peaking at 711  $\text{cm}^{-1}$  for ( $x = 0.03$ ) whereas the heaviest one  $\text{Zn}^{2+}$  responds for the 617  $\text{cm}^{-1}$  modes. Because the iron possesses an intermediate-mass, we have associated the 621  $\text{cm}^{-1}$  modes for the  $\text{Fe}^{3+}$  ion in the tetrahedral sublattice to see the inset on from (Fig. 3.4), it is observed in the spectra changes in the relative intensities of the peaks belonging to each ion. Following Wang Z et al., thus it is clear that Mn, Fe, and Zn ions are present in both sites of the spinel structure.

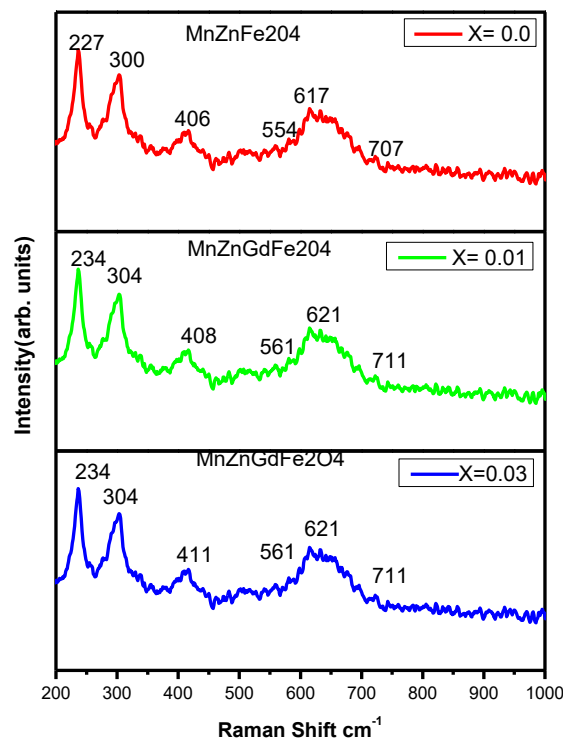


**Figure 3.4:** Raman spectra of nano crystalline  $\text{MnZn}_x\text{Gd}_x\text{Fe}_{2-x}\text{O}_4$ , ( $x = 0.00, 0.01, 0.03$ )

#### 4. Conclusion

It is found that the combustion of manganese nitrate, zinc nitrates and iron nitrate with citric acid results in a series of mixtures of new phases, which convert to  $\text{MnZnFe}_2\text{O}_4$  spinel phase during subsequent heat treatment pre-sintering at 500 °C and sintered at 1250 °C. The results also show that the combustion synthesis of  $\text{MnZnFe}_2\text{O}_4$  can efficiently induce a redistribution of divalent and trivalent ions in the A and B sites.  $\text{MnFe}_2\text{O}_4$  ferrite was synthesized by calcination at various temperatures. The manganese ferrite formed in the cubic spinel structure has been confirmed by the XRD nanoparticle of Gd doped  $\text{Mn}_{0.5}\text{Zn}_{0.5}\text{Gd}_x\text{Fe}_{2-x}\text{O}_4$  spinel ferrites have been synthesized using citrate precursor technique. Crystallite size decreases with an increase in Gd content. XRD studies justify the formation of a cubical spinel structure. Ferrite behavior has been observed for all Gd doped Mn-Zn nano ferrite samples. The cubic spinel structure with a single-phase was revealed by XRD analysis. Scanning electron microscopy was used to study the morphology of prepared  $\text{Mn}_{0.5}\text{Zn}_{0.5}\text{Gd}_x\text{Fe}_{2-x}\text{O}_4$  ferrites. The grains represent well defined faceted and flakes structure. The average particle size of the prepared samples was 14.48 nm. FTIR studies justify the formation of cubical spinel structure and the line width decreases with an increase in Gd content. The FT-IR spectrum shows the most intense absorption bands 451  $\text{cm}^{-1}$  and 655  $\text{cm}^{-1}$  due to the strong transition metal. The Raman results showed the presence of manganese, zinc, and iron ions are present in both side tetrahedral and octahedral sites.  $\text{Mn}^{2+}$  responds for the Raman mode peaking at 711  $\text{cm}^{-1}$ ,  $\text{Zn}^{2+}$  responds for the 617  $\text{cm}^{-1}$  modes at ( $x=0.01$ ) and  $\text{Fe}^{3+}$  ion in the tetrahedral sublattice for the mode 621  $\text{cm}^{-1}$ .

#### References:

1. R.Arulmurugana, B.Jeyadevanb, G. Vaidyanathan, S.Sendhilnathanc, Effect of zinc substitution on Co-Zn and Mn-Zn ferrite nanoparticles prepared by co-precipitation, *J. Magn. Mater.* 288 (2005) 470-477.
2. A. Thakur, M.Singh, Preparation and characterization of nanosize  $\text{Mn}_{0.4}\text{Zn}_{0.6}\text{Fe}_2\text{O}_4$  ferrite by citrate precursor method, *Ceram. Int.* 29 (2003) 505-511.
3. U. Ghazanfar, S.A Siddiqi, G.Abbes, Structural analysis of the Mn-Zn ferrites using XRD technique, *Mater. Sci. Eng.* 118 (2005) 84-86.
4. C. Ingo, C.Heck, Magnetic materials and their applications, *J. Appl. Phys.* 199(1974) 212-213.
5. C.Rath, K.K. Shahu, S. Anand, S.K. Date, N.C.Mishra, R.P.Das, Electrical and magnetic properties, *J. Magn.Mater.* 202 (1999) 77-83.
6. W. Katarzyna, S. Irena, K.Roman, Manganese-zinc ferrite synthesis by the sol-gel auto combustion method, *ACS Publication* 52 (2012) 353-361
7. P.G. Partha, A.C. Hanif, C. Sankar, S.M.Vijayanand, Synthesis and characterization of manganese ferrite nanoparticles, *Ind. Eng. Chem. Res.* 52 (2013) 17848-17855.
8. G. Alex, Modern Ferrite Technology electronic materials research scientists and technician's ferrite, *Springer Sci. Rev.* 9 (2006) 438-456.

9. B.Jeyadevan, C.N.Chinnasamy, K. Shinoda, K.Tohji, Mn-Zn ferrite with higher magnetization for temperature-sensitive magnetic fluid, *J. Appl.Phys.* 93 (2003) 8450-8452.
10. J.Azadmanjiri, Preparation of Mn-Zn ferrite nanoparticle from chemical sol-gel combustion method and the magnetic properties after sintering, *J. Non-Cryst. Sol.* 353 (2007) 4170-4173.
11. S.Gubbala, H. Nathani, K. Koizol, R.D.K.Misra, Magnetic properties of nano ferrites synthesized by reverse micelle technique. *Physica, B.* 348 (2004) 317-328.
12. N. Cai, J. Zhai, C.W. Nan, Y. Lin,Z.Shi, Dielectric, ferroelectric, magnetic, and magnetoelectric properties of multiferroic laminated composites, *Phys. Rev. B.* 68 (2003) 224103.
13. C. Rath, S. Anand, K.K. Sahu, S.D.Kulkarni, S.K. Date, N.C.Mishra,Dependence on action distribution of particle size, lattice parameter, and magnetic properties in nanosize Mn-Zn ferrite, *J. Appl. Phys.* 91 (2002) 2211-2215.
14. P. Thakur, R. Sharma, V. Sharma, P.B. Barman, M. Kumar, D. Barman, P.Sharma,Gd<sup>3+</sup> doped Mn-Zn soft ferrite nanoparticle super paramagnetism and its correlation with other physical properties,*J. Magn. Magn.* 432 (2017) 208-217.
15. R. Sharma, R. Thakur, P. Thakur, M. Kumar, N. Thakur, N.S. Negi, P. Sharma, V.Sharma, Improvement in the magnetic behavior of cobalt doped magnesium zinc nano-ferrites via Co-precipitation route, *J. Alloy. Compd.* 684 (2016) 569-581.
16. J. Azadmanjiri, Preparation of Mn-Zn ferrite nanoparticle from chemical sol-gel combustion method and the magnetic properties after sintering. *J. Non-Cryst. Solids.* 353 (2007) 4170-4173.
17. P. Thakur, R. Sharma, M. S.C. Kumar, S.C. Katyal, N. Thakur, S. Vineet, V. Sharma, P.Sharma, Superparamagnetic La-doped Mn-Zn nano ferrites: dependence on dopant content and crystallite size, *Mater. Res. Express*, 3 (2016) 1-6.
18. T. Slatineanu, A.R. Iordan, M.N. Palamaru, O.F. Caltun, V. Gafton, L.Leontie, Synthesis and characterization of nanocrystalline Zn ferrites substituted with Ni, *Mater. Res. Bull.* 46 (2011) 1455-1460.
19. M.A. Gabal, S. Kosa, T.V.A. Mutairi, Structural and magnetic properties of Ni<sub>1-x</sub>Zn<sub>x</sub>Fe<sub>2</sub>O<sub>4</sub> nano-crystalline ferrites prepared via a novel method. *J. Molec. Strut.* 1063 (2014) 269-273.
20. P. Priyadarshini, P.A Pradeep,P.S. Rao, G.Chandrasekaran, Structural, spectroscopic and magnetic studies of nanocrystalline Ni-Zn ferrites. *Mater. Chem. Phys.* 116 (2009) 207-213.
21. R. Gupta, A. Sood, P. Metcalf, J.M. Honig, Raman study of stoichiometric and Zn-doped Fe<sub>3</sub>O<sub>4</sub>. *Phys. Rev. B.* 65 (2002) 1-8.
22. S.D. Silva, F. Nakagomi, M.S. Silva, A.F. Jr, V.K. Garg, A.C. Oliveria, P.C. Morais, Effect of the Zn content in the structural and magnetic properties of Zn<sub>x</sub>Mg<sub>1-x</sub>Fe<sub>2</sub>O<sub>4</sub> mixed ferrites monitored by Raman and Mossbauer spectroscopies. *J Appl Phys.* 107 (2010) 1-4.
23. Z. Wang, D. Schiferl, Y. Zhao, H.S.C.O. Neill, High-pressure Raman spectroscopy of spinel-type ferrite ZnFe<sub>2</sub>O<sub>4</sub>. *J Phys. Chem. Solid.* 64 (2003) 2517-2520.